



## Highly viscous phase behavior of organic-rich urban PM<sub>2.5</sub>

Atta Ullah<sup>1</sup>, Ji Yi Lee<sup>2</sup>, Zhijun Wu<sup>3</sup>, Kyoung-Soon Jang<sup>4</sup>, and Mijung Song<sup>1,5</sup>

<sup>1</sup>Department of Earth and Environmental Sciences, and Earth Environmental System Research Center, Jeonbuk National University, Jeollabuk-do Jeonju-si 54896, Republic of Korea

<sup>2</sup>Department of Environmental Science & Engineering, Ewha Womans University, Seoul 03760, Republic of Korea

<sup>3</sup>State Key Joint Laboratory of Environmental Simulation and Pollution Control, College of Environmental Sciences and Engineering, Peking University, Beijing 100871, China

<sup>4</sup>Bio-Chemical Analysis Team, Korea Basic Science Institute, Cheongju 28119, Republic of Korea

<sup>5</sup>Department of Climate, Environment and Energy, Jeonbuk National University, Jeollabuk-do Jeonju-si 54896, Republic of Korea

**Correspondence:** Mijung Song (mijung.song@jbnu.ac.kr)

Received: 27 January 2026 – Discussion started: 10 February 2026

Revised: 14 April 2026 – Accepted: 12 May 2026 – Published: 27 May 2026

**Abstract.** Atmospheric aerosol viscosity strongly influences particle phase state, internal mixing, and multi-phase chemical processes, yet direct quantitative constraints for ambient urban PM<sub>2.5</sub> remain limited. Here, we investigated the phase behavior and viscosity of organic-rich PM<sub>2.5</sub> samples collected during autumn 2023 from the urban environments of Seoul and Beijing. Using filter extracts, relative humidity (RH)-dependent phase transitions and morphological evolution of the droplets were examined by optical microscopy, revealing frequent two-phase and three-phase morphologies during dehydration. Aerosol viscosity was quantitatively constrained at  $\sim 290$  K under experimentally accessible RH conditions ( $< \sim 45\%$ ) using the poke-and-flow technique coupled with fluid-dynamic simulations, yielding viscosities spanning from  $\sim 10^4$  to  $> \sim 10^8$  Pa s. Compared with previously reported laboratory-based viscosity measurements, the inferred viscosities of ambient PM<sub>2.5</sub> were comparable to or exceeded those reported for organic-rich ternary systems (i.e., sucrose–AS–H<sub>2</sub>O and citric acid–AS–H<sub>2</sub>O), which are commonly used as laboratory proxy systems in aerosol viscosity studies. These results indicate that organic-rich urban PM<sub>2.5</sub> can exhibit highly viscous, semisolid to solid phase states, and they provide quantitative, field-based viscosity estimates constrained by the bulk organic and inorganic mass fractions of urban aerosols. Although based on a limited number of filter samples and analyzed droplets, these findings offer a foundation for future, more extensive viscosity studies of urban aerosols.

### 1 Introduction

Atmospheric fine particulate matter (PM<sub>2.5</sub>) in urban megacities undergoes a range of general physicochemical processes, including hygroscopic growth, phase transitions, viscosity changes, and diffusion-limited internal mixing, which are strongly modulated by relative humidity (RH) (Swietlicki et al., 2008; Guo et al., 2014; Reid et al., 2018; Song et al., 2022; Freedman et al., 2024; Tan et al., 2024). These pro-

cesses play a critical role in gas–particle partitioning (Zuend and Seinfeld, 2012; Zhou et al., 2013; Gkatzelis et al., 2018; Zaveri et al., 2020), heterogeneous chemical reactivity (Li et al., 2020; Rasool et al., 2023; Song et al., 2025), aging dynamics (Shiraiwa et al., 2011; Liu et al., 2025), and cloud formation (Suda et al., 2014; Cheung et al., 2020; Pöhlker et al., 2023), yet their underlying mechanisms remain poorly constrained by empirical observations. This limitation fundamentally undermines the accurate parametrization of urban

aerosol impacts in atmospheric models, for example, by violating the liquid-phase assumptions underlying gas–particle partitioning schemes and heterogeneous reactive uptake coefficients (Shiraiwa and Seinfeld, 2012; Gržinić et al., 2015).

PM<sub>2.5</sub> exerts major influences on air quality, human health, and climate forcing because of its chemical complexity and diverse physical properties (Seinfeld et al., 2016; McNeill, 2017; Su et al., 2020; Nault et al., 2021; Wall et al., 2022; El Haddad et al., 2024; Bei et al., 2025; Manavi et al., 2025). PM<sub>2.5</sub> typically consists of organic aerosols (OA), inorganic salts, trace metals, mineral dust, and elemental or black carbon (EC or BC). Among these components, OA, including primary (POA) and secondary (SOA), have been frequently observed as the dominant fraction across many continental regions, accounting for approximately 20%–90% of total PM<sub>2.5</sub> mass (Kanakidou et al., 2005; Hallquist et al., 2009; Jimenez et al., 2009; Huang et al., 2014; Zhang et al., 2017; Jeon et al., 2023). These OA are chemically complex, encompassing thousands of molecules, and their oxygen-to-carbon elemental ratios (O : C) have been shown to vary with atmospheric processing and environmental conditions (Zhang et al., 2007; Aiken et al., 2008; Canagaratna et al., 2015; An et al., 2019; Daellenbach et al., 2019; Sun et al., 2025; Cai et al., 2026).

Among the physical properties affected by the chemical complexity and atmospheric evolution of PM<sub>2.5</sub>, particle phase state, described in terms of dynamic viscosity, is particularly important for controlling particle reactivity. Viscosity describes the internal resistance of a material to flow or deform, quantifying molecular mobility within the condensed phase. In the atmospheric context, viscosity serves as a critical indicator of particle phase state: aerosols with dynamic viscosities below 10<sup>2</sup> Pa s behave as liquids, those between 10<sup>2</sup> and 10<sup>12</sup> Pa s are considered as amorphous semisolids, and particles exceeding 10<sup>12</sup> Pa s are considered as amorphous solids (Koop et al., 2011; Zobrist et al., 2008). A highly viscous particle restricts internal diffusion and slows multiphase chemistry, whereas low-viscosity liquid-like particles facilitate rapid gas–particle exchange and aging (Kuwata and Martin, 2012; Berkemeier et al., 2014; Gou et al., 2025).

During the past decade, extensive laboratory studies have attempted to quantify aerosol viscosity using organic or mixed organic–inorganic systems (Renbaum-Wolff et al., 2013a; Song et al., 2016b; Marshall et al., 2018; Rovelli et al., 2019; Jeong et al., 2022; Tong et al., 2022; Mahant et al., 2023; Sheldon et al., 2023; Gou et al., 2025). Measurements for SOA derived from anthropogenic (i.e., toluene, diesel fuel vapors, and phenolic compounds) and biogenic (i.e., isoprene,  $\alpha$ -pinene,  $\beta$ -ocimene, limonene,  $\beta$ -caryophyllene, and valencene) precursors have revealed that viscosity can span more than ten orders of magnitude, from 10<sup>−3</sup> Pa s under humid conditions to over  $\sim$  10<sup>8</sup> Pa s at low RH (Renbaum-Wolff et al., 2013b; Grayson et al., 2016; Hinks et al., 2016; Song et al., 2016a, 2019; Ullmann et al., 2019; Maclean et

al., 2021; Smith et al., 2021; Baboosian et al., 2022; Nikkho et al., 2024; Liu et al., 2026). These findings demonstrate that aerosol viscosity depends strongly on chemical composition, including the organic-to-inorganic mass ratio (OIR), RH, and temperature. However, almost all such data have been derived from laboratory-generated SOA or proxy mixtures, rather than real ambient particles.

Seoul and Beijing represent typical urban environments influenced by mixed anthropogenic emissions, where PM<sub>2.5</sub> is frequently dominated by OA and secondary inorganic aerosols (SIA) (Son et al., 2012; Tao et al., 2017; Kim et al., 2018, 2022; Zhou et al., 2020; Qiu et al., 2023; Cheng et al., 2024b; Daellenbach et al., 2024). Field studies have shown that OA frequently contributes more than half of the PM<sub>2.5</sub> mass in Seoul and Beijing and comprises a mixture of POA (traffic, cooking, biomass, or coal/solid-fuel combustion) and SOA formed from various precursors under a range of meteorological conditions (Sun et al., 2010; Hu et al., 2017; Kim et al., 2017; Zhao et al., 2019; Qiu et al., 2023; Cheng et al., 2024b). In such OA-rich urban environments, the phase state and viscosity of PM<sub>2.5</sub> are expected to be strongly controlled by the properties of the organic fraction, with direct implications for hygroscopic growth, gas–particle partitioning, and particle diffusion (Shiraiwa et al., 2011; Davies and Wilson, 2015; Hosny et al., 2016; Tong et al., 2022). Consequently, direct constraints on the phase state and viscosity of urban OA-containing PM<sub>2.5</sub> remain essential for interpreting PM<sub>2.5</sub> composition and reducing uncertainties in process-level air-quality assessments.

In this study, PM<sub>2.5</sub> samples were collected from the urban environments of Seoul and Beijing during autumn 2023. The samples were characterized by high organic mass fractions, representing organic-rich urban aerosols. Using filter extracts, we investigated RH-dependent phase behavior and morphological evolution using optical microscopy. We then quantitatively constrained aerosol viscosity at a temperature of  $\sim$  290 K under experimentally accessible RH conditions ( $<$   $\sim$  45%) using the poke-and-flow technique. Finally, we compared the determined viscosities with those reported in previous laboratory studies of organic–inorganic aerosol systems. By providing direct quantitative viscosity data for field-collected PM<sub>2.5</sub> in urban environments, this work advances our understanding of the physicochemical behavior of ambient aerosols in the real atmosphere.

## 2 Experimental and methods

### 2.1 Measurement sites and collection of PM<sub>2.5</sub> samples

PM<sub>2.5</sub> sampling was conducted at an urban environmental monitoring station in Bulgwang-dong, Seoul (37.61° N, 126.93° E) and the Changping campus of Peking University, Beijing (40.25° N, 116.19° E). Both sites are located in densely populated metropolitan areas characterized by heavy traffic and significant industrial activity, making them repre-

sentative of typical urban environments. At each site, a total of three PM<sub>2.5</sub> samples were collected on quartz-fiber filters (20.3 × 25.4 cm, Pall Corporation, 7204) over the sampling period between September and October 2023. Each sample was collected from 10:00 to 09:00 LT using a high-volume sampler operating at approximately 1000 L min<sup>-1</sup> (SIBATA HV-1000R, Japan). During the sampling period, the average ambient RH and temperature were 69 ± 12 % and 290 ± 4 K at the Seoul site, and 54 ± 13 % and 293 ± 4 K at the Beijing site, respectively.

After collection, filters were individually sealed in aluminum foil, placed in zip-lock bags, and stored at ~ 255 K to minimize evaporative loss of semi-volatile compounds and microbial degradation. All morphology and viscosity experiments were conducted within ~ 1 month of collection to limit changes in PM<sub>2.5</sub> chemical and physical properties. For the morphology and viscosity experiments, PM<sub>2.5</sub> material was recovered from each filter using a 1 : 1 (*v/v*) methanol–water extraction procedure designed to capture both hydrophilic and hydrophobic species, as detailed in Sect. S1 in the Supplement. The resulting extract was then nebulized onto a hydrophobic glass substrate (Hampton Research, Canada) using a nebulizer (MEINHARD, PerkinElmer, USA) to generate PM<sub>2.5</sub> droplets. Details of the methods used to determine chemical compositions are provided in Sect. S2.

## 2.2 Observation of morphological change upon dehydration

To investigate morphological changes of the PM<sub>2.5</sub> droplets on a hydrophobic substrate, optical microscopy was employed following the approach used in previous studies (Ham et al., 2019; Jeong et al., 2022; Song et al., 2022; Seong et al., 2024). Briefly, PM<sub>2.5</sub> droplets were first equilibrated at ~ 100 % RH and 290 ± 1 K for ~ 20 min in an RH- and temperature-controlled flow-cell (TSA12Gi, Instec, USA), and then the RH was reduced at a rate of 0.5 % RH min<sup>-1</sup> down to ~ 0 % RH. During typical experiments, the morphological evolution of the droplets before, during, and post-poking was monitored via optical microscopy (Olympus BX43, 40× objective, Japan) and recorded with a CCD camera (DigiRetina 16, Tucsen, China). The RH sensor (Sensirion, SHT C3, Switzerland) within the flow-cell was calibrated at 290 K using deliquescence RH of K<sub>2</sub>CO<sub>3</sub> (44 % RH), NaCl (76 % RH), and (NH<sub>4</sub>)<sub>2</sub>SO<sub>4</sub> (80 % RH) (Winston and Bates, 1960), with an associated uncertainty of ± 1.5 %. RH control was achieved by adjusting the mixing ratio of dry N<sub>2</sub> and H<sub>2</sub>O-saturated vapor at a constant total flow rate of 500 sccm. The experimental temperature (290 K) was selected to closely reflect the average conditions at the sampling sites, thereby ensuring environmental relevance.

## 2.3 Poke-and-flow technique

The poke-and-flow technique was employed to determine the viscosity of highly viscous PM<sub>2.5</sub> droplets on a hydrophobic substrate within a temperature- and RH-controlled flow-cell (Renbaum-Wolff et al., 2013b; Grayson et al., 2015; Song et al., 2015, 2025). In this technique, a micrometer-scale droplet (~ 20–40 μm in diameter) is mechanically deformed by a fine needle; the subsequent relaxation of the deformed shape is governed by the competition between surface tension (restoring force) and viscous resistance, allowing viscosity to be quantified from the observed relaxation timescale in combination with fluid-dynamics simulations (Sect. 2.4). The morphological evolution of the droplets before, during, and after poking was monitored using optical microscopy (Olympus CKX53 with a 40× objective, Japan) and recorded with a CCD camera (Hamamatsu, C11440-42U30, Japan).

For viscosity measurements, droplets were first equilibrated at ~ 100 % RH, then RH was decreased to ~ 40 % at ~ 1 % RH min<sup>-1</sup>. Poking was performed at RH levels of ~ 40 %, ~ 30 %, ~ 20 %, ~ 10 %, and ~ 0 % using a fine needle (Jung Rim Medical Industrial, South Korea) mounted on a micromanipulator (Narishige, model MO-152, Japan). Before each poking, droplets were conditioned for ~ 1 h at the target RH to ensure equilibration, consistent with previous studies on semisolid particles (Kiland et al., 2023; Gerrebos et al., 2024; Ullah et al., 2026). Following poking, a hole formed and gradually closed; the time required for the equivalent hole diameter to decrease to 50 % of its initial value was defined as the experimental flow time,  $\tau_{(\text{exp, flow})}$  (see Sect. 2.4 for details). In typical experiments, one to five particles per sample were analyzed at each RH, and the total number of droplets analyzed per sample ranged from one to nine. At RH > ~ 50 %, the PM<sub>2.5</sub> droplets behaved as low-viscosity liquids and hole closure occurred too quickly to be captured within the imaging frame rate; therefore,  $\tau_{(\text{exp, flow})}$  could not be determined under these conditions.

## 2.4 Fluid-dynamic simulations

Viscosities were determined from  $\tau_{(\text{exp, flow})}$  using finite-element fluid flow simulations in COMSOL Multiphysics (version 5.5), employing the Laminar Flow and Moving Mesh interfaces to model viscous droplet flow and droplet geometry deformation during relaxation, respectively, following established methods (Renbaum-Wolff et al., 2013b; Grayson et al., 2015; Song et al., 2015, 2016a). In the simulations, the poked droplet was represented as a half-torus geometry, with the inner and outer diameters determined from optical images acquired after poking. Since the inner hole could exhibit irregular, non-axisymmetric shapes, its perimeter was traced from the optical images, the enclosed area was calculated, and an equivalent circular diameter ( $d = (4A/\pi)^{1/2}$ ) was used to define the initial torus geometry and  $\tau_{(\text{exp, flow})}$ . For each particle for which flow was observed, the

dynamic viscosity was iteratively adjusted until  $\tau_{(\text{model, flow})}$  agreed with  $\tau_{(\text{exp, flow})}$  to within  $\sim 1\%$  (Song et al., 2016a).

The key physical parameters required for the simulations, along with their lower- and upper-bound values, are summarized in Table 1. The slip length, which characterizes the degree of velocity slip at the fluid–solid interface, was bounded between 5 nm and 10  $\mu\text{m}$  based on literature values for fluid–solid interactions at hydrophobic surfaces (Schnell, 1956; Churaev et al., 1984; Watanabe et al., 1999; Baudry et al., 2001; Cheng and Giordano, 2002; Tretheway and Meinhart, 2002; Jin et al., 2004; Joseph and Tabeling, 2005; Choi and Kim, 2006; Zhu et al., 2012; Li et al., 2014). For density and surface tension, bounds were selected based on representative aerosol types: the lower bound used properties of isoprene-derived SOA (density: 1.2  $\text{g cm}^{-3}$ , Li et al., 2022; surface tension: 17  $\text{mN m}^{-1}$ , <https://www.chemspider.com/>, last access: 1 December 2025), and the upper bound applied values for supersaturated ammonium sulfate (AS) (density: 1.7  $\text{g cm}^{-3}$ , <https://www.chemspider.com/>, last access: 1 December 2025; surface tension: 95  $\text{mN m}^{-1}$ , Mikhailov et al., 2024). Although the sampled PM<sub>2.5</sub> is predominantly organic, inorganic salts such as AS can become highly concentrated under dry conditions and strongly inhibit particle flow, providing a conservative upper viscosity limit. Contact angles were determined from side-view optical images of representative droplets on the substrate using ImageJ (Grayson et al., 2015), with measured values ranging from 30 to 75°, reflecting variability in droplet size and composition across the analyzed samples. The overall uncertainty of approximately two orders of magnitude in the derived viscosity stems from the variability in these input parameters, with the slip length being the primary contributor (Grayson et al., 2015; Song et al., 2015).

At low RH, droplets exhibited brittle cracking without relaxation, indicating non-flowing behavior. If no recovery was observed over  $\sim 2\text{ h}$ , a lower-bound viscosity of  $\sim 1 \times 10^8\text{ Pa s}$  was assigned, following established practice in poke-and-flow studies (Renbaum-Wolff et al., 2013b; Jeong et al., 2022; Gerrebos et al., 2024, 2025).

### 3 Results and discussion

#### 3.1 Chemical characteristics of PM<sub>2.5</sub>

The chemical composition of PM<sub>2.5</sub> collected from Seoul and Beijing during autumn 2023 is summarized in Fig. S2 and Table 2. The major components include organic matter (OM), sulfate, nitrate, ammonium, and minor ions (e.g.,  $\text{K}^+$ ,  $\text{Na}^+$ ,  $\text{Ca}^{2+}$ ,  $\text{Mg}^{2+}$ , and  $\text{Cl}^-$ ). OM consistently accounted for more than  $\sim 65\%$  of the total PM<sub>2.5</sub> mass across all the samples. Although this classification captures the dominant aerosol constituents, trace species such as metals, black carbon, and crustal materials also contribute to PM<sub>2.5</sub> but were not the focus of this study.

The daily PM<sub>2.5</sub> concentrations at the Seoul and Beijing sites ranged from  $\sim 7.0$  to 31.7  $\mu\text{g m}^{-3}$ , encompassing both relatively clean and polluted conditions based on the World Health Organization (WHO) 24-hour air quality guideline of 15  $\mu\text{g m}^{-3}$  (World Health Organization, 2021). Over this range, the OIR varied from approximately 2 : 1 to 8 : 1, consistent with values commonly observed in various tropospheric environments (Hodzic et al., 2020; Cheng et al., 2024a; Zhang et al., 2024).

The bulk O : C ratios ( $\sim 0.4$ – $0.5$  at both sites, Table 2) fall within the typical range for urban OA (Aiken et al., 2008; Chen et al., 2015; Zhou et al., 2020), indicating that the organics were overall moderately oxidized. This composition suggests a substantial fraction of hydrophilic, highly oxygenated secondary organics alongside a non-negligible pool of more hydrophobic, less oxidized material (Kim et al., 2025). Consequently, autumn-time OM in Seoul and Beijing can be characterized as an amphiphilic mixture, consistent with previous mass spectrometric observations of urban aerosols in the region (Kim et al., 2022). Although inorganic ions were not the dominant mass component as reflected by the OIR ranges (Table 2), they still represented an important fraction of PM<sub>2.5</sub>, primarily as SIA dominated by ammonium sulfate (AS) with additional contributions from ammonium nitrate (AN) (Fig. S2; Sect. S2).

#### 3.2 Morphological characteristics and phase behavior of PM<sub>2.5</sub> droplets

To directly observe the phase behavior under progressively lowering RH, micrometer-sized droplets generated from PM<sub>2.5</sub> extracts were monitored in a temperature- and RH-controlled flow-cell at  $290 \pm 1\text{ K}$ . This temperature closely matches the mean ambient conditions during the autumn sampling period at both sites (Seoul:  $290 \pm 4$ ; Beijing:  $293 \pm 4\text{ K}$ ; Table 2). Figure 1 shows optical images at four RH levels ( $\sim 95\%$ ,  $\sim 85\%$ ,  $\sim 60\%$ , and  $\sim 20\%$ ), illustrating the evolution of particle morphology and phase state during dehydration. At high RH ( $\sim 95\%$ ), droplets behaved as a homogeneous single-phase liquid. They appeared smooth and rounded, with uniform optical contrast and no discernible internal structure, indicating that near water saturation, the urban PM<sub>2.5</sub> extracts form well-mixed single-phase liquid.

As RH decreased to  $\sim 85\%$ , all droplets exhibited internal structuring consistent with liquid-liquid phase separation (LLPS) (Ciobanu et al., 2009; Song et al., 2012; Freedman, 2017; Ham et al., 2019; Lam et al., 2021; Freedman et al., 2024). Because the droplets remained single phase at  $\sim 95\%$  RH but had clearly phase-separated by  $\sim 85\%$  RH, the observed separation RH in our experiments was constrained to between  $\sim 95\%$  and  $\sim 85\%$  RH. Distinct inner and outer regions emerged, often accompanied by small inclusions or domains within the droplet. These two-phase liquid morphologies adopted a core–shell geometry (Fig. 1), consistent with LLPS behavior established in

**Table 1.** Summary of the key input physical parameters and boundary conditions used in the COMSOL Multiphysics simulations for the lower- and upper-bound viscosity calculations.  $R$  and  $r$  denote the geometric parameters of the torus: Here,  $R$  is the distance from the center of the hole to the midpoint of the torus ring, and  $r$  is the radius of the torus ring.

Parameter	Lower-bound calculation	Upper-bound calculation
Slip length <sup>a</sup>	5 nm	10 μm
Density <sup>b</sup>	1.2 g cm <sup>-3</sup>	1.7 g cm <sup>-3</sup>
Surface tension <sup>c</sup>	17 mN m <sup>-1</sup>	95 mN m <sup>-1</sup>
Contact angle	30° ( $r < 2R$ ), 75° ( $r > 2R$ )	75° ( $r < 2R$ ), 30° ( $r > 2R$ )

<sup>a</sup> The slip length is based on values reported in the literature for fluid–solid interactions at hydrophobic surfaces (Schnell, 1956; Churaev et al., 1984; Watanabe et al., 1999; Baudry et al., 2001; Cheng and Giordano, 2002; Tretheway and Meinhart, 2002; Jin et al., 2004; Joseph and Tabeling, 2005; Choi and Kim, 2006; Zhu et al., 2012; Li et al., 2014). <sup>b</sup> Values taken from Li et al. (2022) and <https://www.chemspider.com/> (last access: 1 December 2025). <sup>c</sup> Values taken from <https://www.chemspider.com/> (last access: 1 December 2025) and Mikhailov et al. (2024).

**Table 2.** Summary of mean ambient temperature, relative humidity (RH), mass concentration of PM<sub>2.5</sub>, and sulfate, nitrate, ammonium, and minor ions (K<sup>+</sup>, Na<sup>+</sup>, Ca<sup>2+</sup>, Mg<sup>2+</sup>, and Cl<sup>-</sup>) in Seoul and Beijing. The mean concentration of organic material (OM) was determined by subtracting the inorganic salts, including sulfate, nitrate, ammonium, and minor ions, from the PM<sub>2.5</sub> mass concentration. OIR refers to the organic-to-inorganic mass ratio, whereas O : C means oxygen-to-carbon elemental ratio. The last column shows the total number of droplets analyzed by the poke-and-flow technique for each sample.

Sampling date (mm dd <sup>-1</sup> )	Ambient temperature (K)	Ambient RH (%)	PM <sub>2.5</sub> (μg m <sup>-3</sup> )	SO <sub>4</sub> <sup>2-</sup> (μg m <sup>-3</sup> )	NO <sub>3</sub> <sup>-</sup> (μg m <sup>-3</sup> )	NH <sub>4</sub> <sup>+</sup> (μg m <sup>-3</sup> )	Minor (μg m <sup>-3</sup> )	OM (μg m <sup>-3</sup> )	OIR	O : C	# of particles
Seoul											
09/30	291 ± 4	76 ± 6	16.8	2.2	0.6	0.9	0.3	12.9	3 : 1	0.45	7
10/12	290 ± 6	62 ± 13	16.4	1.9	1.0	1.0	0.2	12.3	3 : 1	0.47	9
10/15*	287 ± 4	84 ± 6	23.0	3.2	2.2	1.6	0.5	15.5	2 : 1	0.45	2
Beijing											
09/21	296 ± 2	61 ± 8	16.5	1.3	0.3	0.3	0.1	14.6	8 : 1	0.50	6
10/03	293 ± 3	61 ± 6	31.7	2.5	3.8	1.5	0.7	23.1	3 : 1	0.48	1
10/14*	289 ± 5	47 ± 15	7.0	1.0	0.7	0.3	0.3	4.7	3 : 1	0.52	3

\* Samples already reported by Song et al. (2025).

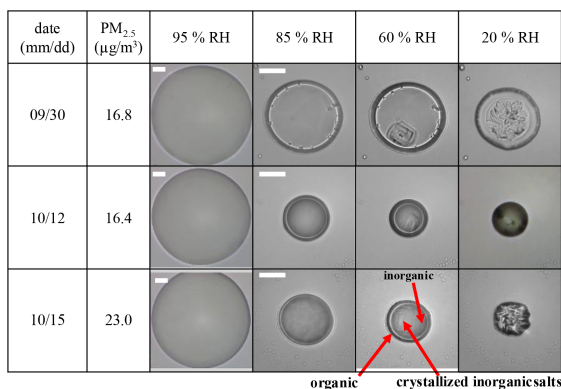
laboratory studies of mixed organic–inorganic particles and with the bulk composition of our samples (O : C = 0.45–0.52; OIR = 2 : 1–8 : 1), for which LLPS is expected based on the O : C threshold of  $\sim 0.80$  below which phase separation commonly occurs in organics mixed with inorganic salts such as AS or AN (Song et al., 2013; You et al., 2013; Stewart et al., 2015; Kucinski et al., 2021; Huang et al., 2024).

Further dehydration to  $\sim 60\%$  RH frequently produced three-phase morphologies. In this regime, solid-like domains coexisted with two liquid regions. Some solid-like inclusions appeared angular (Fig. 1), suggesting crystallized inorganic salts or less soluble organic materials. Based on the bulk ionic composition (dominated by secondary inorganic salts such as AS; Fig. S2 and Sect. S2), it is plausible that at least part of the solid-like material was inorganic-rich, though contributions from non-crystalline organic-rich phases cannot be excluded. The relative volumes of the inner liquid, outer shell, and crystalline regions varied among droplets, reflect-

ing compositional differences and drying history. These observations align with recent laboratory studies showing that mixed organic–inorganic aerosols can exhibit complex multiphase behavior across wide RH ranges (Huang et al., 2021).

At low RH ( $\sim 20\%$ ), most droplets transitioned to non-liquid morphologies. Droplets displayed features characteristic of efflorescence, either confined to the inner region or involving nearly the entire particle (Fig. 1). These observations indicate that at least one phase had effectively lost its ability to flow, consistent with the presence of effloresced inorganic solids and/or highly viscous organic material. Because morphology alone cannot unambiguously distinguish crystalline solids from extremely viscous amorphous semisolids, these low-RH states are treated as non-liquid. Quantitative viscosity of the bulk of PM<sub>2.5</sub> is provided by poke-and-flow measurements in Sect. 3.3.

## (a) Seoul



## (b) Beijing

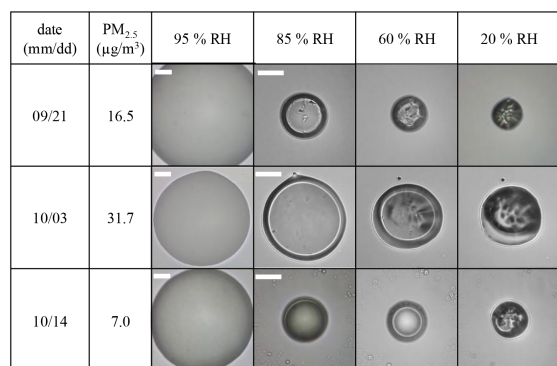


**Figure 1.** Optical images obtained during RH decrease for (a) Seoul and (b) Beijing PM<sub>2.5</sub> droplets showing phase separation, as RH decreases from ~95 % to 85 %, 60 %, and 20 %. Upon dehydration, particles transition from a homogeneous single-phase liquid to a core-shell morphology, illustrating separation of organic and inorganic components driven by water loss. The images at ~95 % RH are shown at the same scale, while those at ~85 % RH and lower are presented at a consistent scale to facilitate comparison between samples. The scale bar represents 20 μm. Seoul (10/15) and Beijing (10/14) samples have already been reported by Song et al. (2025) and are included here for completeness of discussion.

### 3.3 Viscosity and phase state of organic-rich PM<sub>2.5</sub>

To quantitatively constrain the RH-dependent viscosity of the bulk of the organic-rich urban PM<sub>2.5</sub>, poke-and-flow experiments were conducted, and the resulting  $\tau_{(\text{exp, flow})}$  values (Fig. S1) were analyzed in combination with fluid-dynamic simulations using COMSOL Multiphysics. Representative optical images of the poke-and-flow experiments are shown in Fig. 3. Previous field studies of ambient PM<sub>2.5</sub> have primarily focused on qualitative phase-state classifications (e.g., liquid, semisolid, or solid) (Bateman et al., 2016; Song et al., 2022; Meng et al., 2024; Seong et al., 2024). However, quantitative, RH-resolved viscosity measurements for urban aerosols remain scarce.

Figure 2 shows the viscosities of PM<sub>2.5</sub> droplets collected from Seoul and Beijing within the experimentally accessi-

ble RH range (RH < ~45 %). Across the RH range between ~45 % and 25 %, the mean viscosities were approximately 10<sup>4</sup>–10<sup>8</sup> Pa s, corresponding to consistencies ranging from peanut butter to tar pitch (Koop et al., 2011; Reid et al., 2018). The autumn-time urban PM<sub>2.5</sub> droplets examined here predominantly fell within the semisolid regime in the studied RH ranges.

Although the poke-and-flow experiments were conducted under drier conditions (RH < ~45 %) than the mean ambient RH during sampling (Seoul: 69 ± 12 %; Beijing: 54 ± 13 %), direct quantitative viscosity constraints at higher RH could not be obtained, as the droplets behaved as low-viscosity liquids above ~45 % RH and relaxed too rapidly to yield a resolvable  $\tau_{(\text{exp, flow})}$ . Nevertheless, comparison with sucrose–AS–H<sub>2</sub>O systems (Fig. 5) indicates that semisolid behavior may still occur during at least episodic portions of the sampling period, particularly for the Beijing samples and during lower-RH periods in Seoul. These results, therefore, suggest that semisolid behavior of urban PM<sub>2.5</sub> cannot be ruled out even under the RH ambient conditions observed during the sampling period, particularly during drier episodes, and that viscosity measurements at higher RH remain an important target for future work. The derived viscosities exhibited substantial sample-to-sample and droplet-to-droplet variability. The observed spread in  $\tau_{(\text{exp, flow})}$  between individual droplets from the same filter extract likely reflects variability in local phase state upon dehydration, differences in the RH threshold at which inorganic salts become supersaturated, and minor experimental factors such as droplet size heterogeneity, all of which can strongly influence viscosity at intermediate RH.

At lower RH, PM<sub>2.5</sub> droplets frequently exhibited brittle cracking without observable relaxation (Fig. 4). When no restorative flow was detected over observation periods exceeding two hours, a conservative lower-limit viscosity of ~10<sup>8</sup> Pa s was assigned, consistent with the practical lower limit that can be constrained using the poke-and-flow technique (Renbaum-Wolff et al., 2013b; Grayson et al., 2015; Jeong et al., 2022; Gerrebos et al., 2024). Under these conditions, PM<sub>2.5</sub> droplets from Seoul exhibited cracking at RH values of ~9.2 %, ~9.2 %, and ~11.7 %, whereas droplets from Beijing cracked at comparatively higher and more variable RH values of ~18.8 %, ~9.6 %, and ~20.1 % on each date. These observations indicate that the RH threshold for the transition to non-flowing behavior is dependent on PM<sub>2.5</sub> composition. The inferred lower-bound viscosities correspond to consistencies comparable to, or exceeding, those of tar-like materials, suggesting extremely viscous properties or arrested internal flow under dry conditions.

The autumn PM<sub>2.5</sub> samples examined here were overall organic-rich, with sulfate as the dominant inorganic ion, primarily present as AS (Sect. 3.1). The RH-resolved viscosities measured for PM<sub>2.5</sub> were compared with laboratory measurements for internally mixed organic–AS systems, commonly used as surrogates for organic-rich, sulfate-

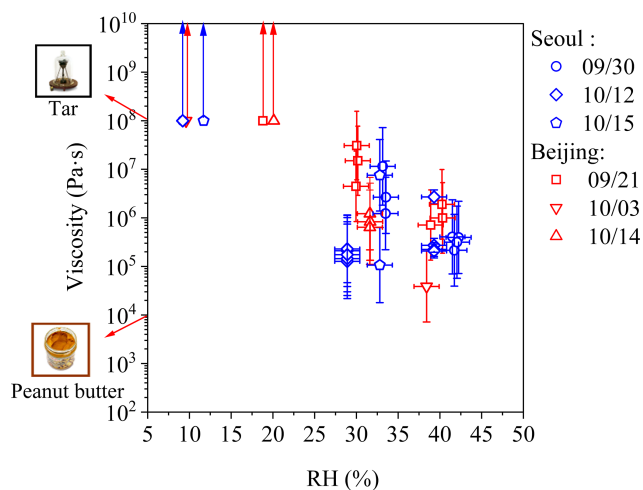


**Figure 2.** Mean viscosities of PM<sub>2.5</sub> droplets derived from experimentally measured flow times (Fig. S1) using poke-and-flow measurements and COMSOL simulations. Markers denote mean values, with  $y$ -error bars indicating upper and lower bound deviations from the mean, calculated as the difference between the mean and the corresponding upper and lower bounds derived from simulations using minimum and maximum input parameters (Table 1). Upward arrows indicate lower-limit viscosities where no restorative flow was observed within the experimental timescale. The  $x$ -axis error bars represent the RH sensor uncertainty ( $\pm 1.5\%$ ), as determined from our RH sensor calibration in the flow-cell (Sect. 2.2). Reference viscosities for peanut butter ( $\sim 10^4$  Pa s) and tar ( $\sim 10^8$  Pa s) are shown for comparison (Koop et al., 2011; Reid et al., 2018).

containing aerosols (Fig. 5). Previous laboratory studies indicated that citric acid (CA)–AS–H<sub>2</sub>O systems exhibited relatively low viscosities and weak RH dependence at comparable RH, whereas sucrose–AS–H<sub>2</sub>O systems showed a pronounced increase in viscosity upon dehydration, reaching  $\sim 10^3$ – $10^5$  Pa s at RH of  $\sim 20\%$ – $30\%$  and approaching  $\sim 10^8$  Pa s upon cracking at lower RH (e.g., sucrose–AS–H<sub>2</sub>O for 4 : 1 and 1 : 1, Fig. 5) (Jeong et al., 2022; Tong et al., 2022; Sheldon et al., 2023). Accordingly, sucrose–AS systems represent the highest RH-dependent viscosities reported among commonly used laboratory surrogates, providing an appropriate upper reference for comparison with organic-rich urban PM<sub>2.5</sub>.

Within the experimentally accessible RH range ( $< \sim 45\%$ ) in this study using the poke-and-flow technique, the viscosities determined for organic-rich urban PM<sub>2.5</sub> droplets were comparable to the highest values reported for sucrose–AS laboratory systems and, in several cases, exceeded this upper range, while remaining consistently higher than those reported for CA–AS systems at comparable RH. These results suggest that organic-rich urban PM<sub>2.5</sub> can attain viscosities at least as high as those of the most viscous laboratory surrogate systems commonly used in aerosol research.

### (a) Seoul

Date (mm/dd)	PM <sub>2.5</sub> ( $\mu\text{g}/\text{m}^3$ )	RH	Pre-poking	Poking	First frame post-poking	$\tau_{(\text{exp. flow})}$ frame post-poking
09/30	16.8	$\sim 40\%$				0 sec, 97 sec
10/12	16.4	$\sim 40\%$				0 sec, 13 sec
10/15	23.0	$\sim 33\%$				0 sec, 48 sec

### (b) Beijing

Date (mm/dd)	PM <sub>2.5</sub> ( $\mu\text{g}/\text{m}^3$ )	RH	Pre-poking	Poking	First frame post-poking	$\tau_{(\text{exp. flow})}$ frame post-poking
09/21	16.5	$\sim 40\%$				0 sec, 251 sec
10/03	31.7	$\sim 40\%$				0 sec, 15 sec
10/14	7.0	$\sim 31\%$				0 sec, 148 sec

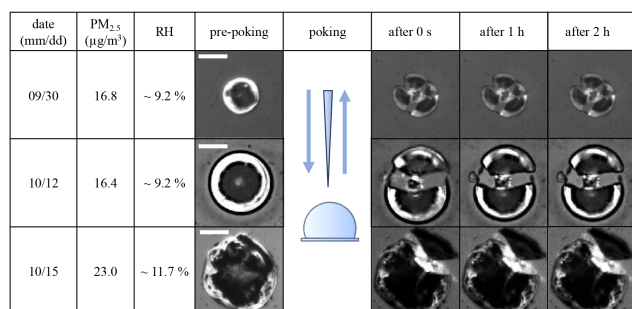
**Figure 3.** Poke-and-flow results for (a) Seoul and (b) Beijing PM<sub>2.5</sub> droplets at  $\sim 40\%$  RH– $\sim 30\%$  RH conditions under which particle flow was observed. The first post-poking frame corresponds to the image taken immediately after needle retraction ( $t = 0$  sec), and the later frame corresponds to the experimental flow time,  $\tau_{(\text{exp. flow})}$ , when the inner hole diameter has decreased to 50% of its initial size. The scale bar represents 20  $\mu\text{m}$ .

Our conclusions are based on a limited number of filters and droplets, and the experiments were conducted on micrometer-sized extracted droplets on a substrate, which may not fully represent submicron ambient particles. Future studies extending viscosity measurements to a larger number of samples across different seasons and to smaller, atmospherically relevant particle sizes would further constrain the phase behavior of urban PM<sub>2.5</sub> under real atmospheric conditions.

## 4 Conclusions

In this study, we investigated the phase behavior and viscosity of organic-rich urban PM<sub>2.5</sub> collected during autumn from Seoul and Beijing, using filter extracts. Optical microscopy observations qualitatively revealed RH-driven phase transitions in all analyzed samples during dehydration, including well-mixed single-phase liquid, two-phase liquid and three-phase morphologies, followed by the development of non-flowing morphologies at lower RH. Using the poke-and-flow

## (a) Seoul



## (b) Beijing

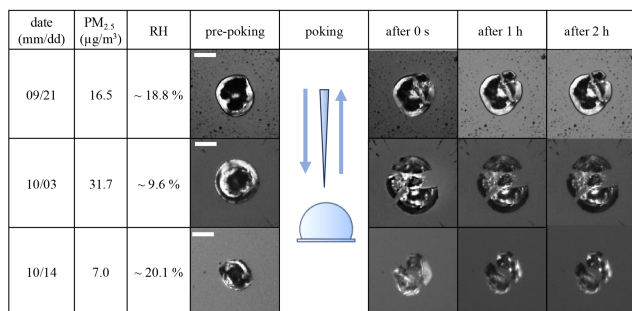


**Figure 4.** Optical images of (a) Seoul and (b) Beijing PM<sub>2.5</sub> droplets exhibiting cracking at their respective RH after poking. The scale bar represents 20 μm.

technique coupled with fluid-dynamic simulations, we quantitatively constrained aerosol viscosity at ~290 K within the experimentally accessible RH range (RH < ~45 %). For ~45 % RH–25 % RH, the inferred viscosities of organic-rich PM<sub>2.5</sub> spanned approximately 10<sup>4</sup>–10<sup>8</sup> Pa s, corresponding to semisolid to non-flowing behavior on the experimental timescale. At lower RH, brittle cracking without observable relaxation was observed, and conservative lower-limit viscosities of ~10<sup>8</sup> Pa s were assigned.

When placed in the context of existing laboratory studies, the viscosities inferred for organic-rich urban PM<sub>2.5</sub> were comparable to the highest values reported for sucrose–AS–H<sub>2</sub>O laboratory systems and, in several cases, exceeded this upper range within the RH interval of 20 %–45 %, while remaining consistently higher than those reported for CA–AS systems at similar RH. These findings demonstrated that organic-rich urban PM<sub>2.5</sub> can attain viscosities at the upper end of RH-dependent viscosity values previously reported for laboratory-generated organic–inorganic aerosol surrogates. Although these constraints were derived from micrometer-sized filter extract droplets and therefore do not fully preserve the native morphology or size of ambient sub-micron particles, they provide direct, field-based quantitative benchmarks under atmospherically relevant low-RH conditions. Such highly viscous states are expected to slow intraparticle diffusion and inhibit internal mixing, with implications for gas–particle partitioning and multiphase chemical

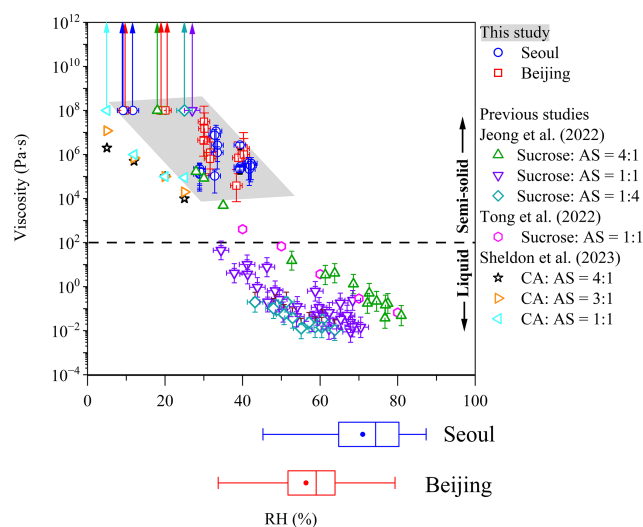


**Figure 5.** RH-dependent viscosities of Beijing and Seoul PM<sub>2.5</sub> droplets compared with sucrose–AS–H<sub>2</sub>O and citric acid (CA)–AS–H<sub>2</sub>O systems from previous studies (Jeong et al., 2022; Tong et al., 2022; Sheldon et al., 2023). Viscosities in the previous studies were determined using the poke-and-flow technique (Jeong et al., 2022), a dual optical tweezer system (Tong et al., 2022), and the droplet coalescence method (Sheldon et al., 2023). *y*-error bars in this study indicate uncertainty ranges of the modeled viscosities for data corresponding to Fig. 2. Box plots in the lower panel show hourly RH distributions in Seoul and Beijing derived from the days on which PM<sub>2.5</sub> samples were collected, with markers indicating mean values, boxes representing the 25th–75th percentiles, and whiskers showing minimum and maximum values.

processing in urban aerosols. However, these conclusions are based on a limited number of filter samples and droplets, and future studies extending measurements across additional seasons, compositions, and particle sizes will be essential for further constraining the role of aerosol viscosity in urban atmospheric processes.

**Data availability.** Underlying material and related data for this paper are provided in the Supplement.

**Supplement.** The supplement related to this article is available online at <https://doi.org/10.5194/acp-26-7311-2026-supplement>.

**Author contributions.** Mijung Song: Conceptualization, Data curation, Funding acquisition, Software, Supervision, Writing–review & editing. Atta Ullah: Data curation, Software, Writing–original draft, Writing–review & editing. Ji Yi Lee: Data curation, Review & editing. Kyoung-Soon Jang: Data curation, Review & editing. Zhijun Wu: Data curation, Review & editing.

**Competing interests.** The contact author has declared that none of the authors has any competing interests.

**Disclaimer.** Publisher's note: Copernicus Publications remains neutral with regard to jurisdictional claims made in the text, published maps, institutional affiliations, or any other geographical representation in this paper. The authors bear the ultimate responsibility for providing appropriate place names. Views expressed in the text are those of the authors and do not necessarily reflect the views of the publisher.

**Acknowledgements.** We thank Daeun Kim for technical support.

**Financial support.** This work was supported by the National Research Foundation of Korea (NRF) grant funded by the Korean government (MSIT) (RS-2024-00335536).

**Review statement.** This paper was edited by Alexander Laskin and reviewed by two anonymous referees.

## References

- Aiken, A. C., DeCarlo, P. F., Kroll, J. H., Worsnop, D. R., Huffman, J. A., Docherty, K. S., Ulbrich, I. M., Mohr, C., Kimmel, J. R., Sueper, D., Sun, Y., Zhang, Q., Trimborn, A., Northway, M., Ziemann, P. J., Canagaratna, M. R., Onasch, T. B., Alfarra, M. R., Prevot, A. S. H., Dommen, J., Duplissy, J., Metzger, A., Baltensperger, U., and Jimenez, J. L.: O/C and OM/OC ratios of primary, secondary, and ambient organic aerosols with high-resolution time-of-flight aerosol mass spectrometry, *Environ. Sci. Technol.*, 42, 4478–4485, <https://doi.org/10.1021/es703009q>, 2008.
- An, Y., Xu, J., Feng, L., Zhang, X., Liu, Y., Kang, S., Jiang, B., and Liao, Y.: Molecular characterization of organic aerosol in the Himalayas: insight from ultra-high-resolution mass spectrometry, *Atmos. Chem. Phys.*, 19, 1115–1128, <https://doi.org/10.5194/acp-19-1115-2019>, 2019.
- Baboomian, V. J., Crescenzo, G. V., Huang, Y., Mahrt, F., Shiraiwa, M., Bertram, A. K., and Nizkorodov, S. A.: Sunlight can convert atmospheric aerosols into a glassy solid state and modify their environmental impacts, *P. Natl. Acad. Sci. USA*, 119, e2208121119, <https://doi.org/10.1073/pnas.2208121119>, 2022.
- Bateman, A. P., Gong, Z., Liu, P., Sato, B., Cirino, G., Zhang, Y., Artaxo, P., Bertram, A. K., Manzi, A. O., and Rizzo, L. V.: Sub-micrometre particulate matter is primarily in liquid form over Amazon rainforest, *Nat. Geosci.*, 9, 34–37, <https://doi.org/10.1038/ngeo2599>, 2016.
- Baudry, J., Charlaix, E., Tonck, A., and Mazuyer, D.: Experimental Evidence for a Large Slip Effect at a Non-wetting Fluid-Solid Interface, *Langmuir*, 17, 5232–5236, <https://doi.org/10.1021/la0009994>, 2001.
- Bei, N., Xiao, B., Wang, R., Yang, Y., Liu, L., Han, Y., and Li, G.: Impacts of aerosol–radiation and aerosol–cloud interactions on a short-term heavy-rainfall event – a case study in the Guanzhong Basin, China, *Atmos. Chem. Phys.*, 25, 10931–10948, <https://doi.org/10.5194/acp-25-10931-2025>, 2025.
- Berkemeier, T., Shiraiwa, M., Pöschl, U., and Koop, T.: Competition between water uptake and ice nucleation by glassy organic aerosol particles, *Atmos. Chem. Phys.*, 14, 12513–12531, <https://doi.org/10.5194/acp-14-12513-2014>, 2014.
- Cai, M., Yuan, B., Hu, W., Chenshuo, Y., Huang, S., Yang, S., Chen, W., Peng, Y., Deng, Z., Zhao, J., Chen, D., Sun, J., and Shao, M.: New insight into the formation and aging processes of organic aerosol from positive matrix factorization (PMF) analysis of ambient FIGAERO-CIMS thermograms, *Atmos. Chem. Phys.*, 26, 769–788, <https://doi.org/10.5194/acp-26-769-2026>, 2026.
- Canagaratna, M. R., Jimenez, J. L., Kroll, J. H., Chen, Q., Kessler, S. H., Massoli, P., Hildebrandt Ruiz, L., Fortner, E., Williams, L. R., Wilson, K. R., Surratt, J. D., Donahue, N. M., Jayne, J. T., and Worsnop, D. R.: Elemental ratio measurements of organic compounds using aerosol mass spectrometry: characterization, improved calibration, and implications, *Atmos. Chem. Phys.*, 15, 253–272, <https://doi.org/10.5194/acp-15-253-2015>, 2015.
- Chen, Q., Heald, C. L., Jimenez, J. L., Canagaratna, M. R., Zhang, Q., He, L. Y., Huang, X. F., Campuzano-Jost, P., Palm, B. B., and Poulain, L.: Elemental composition of organic aerosol: The gap between ambient and laboratory measurements, *Geophys. Res. Lett.*, 42, 4182–4189, <https://doi.org/10.1002/2015GL063693>, 2015.
- Cheng, B., Alapaty, K., and Arunachalam, S.: Spatiotemporal trends in PM<sub>2.5</sub> chemical composition in the conterminous US during 2006–2020, *Atmos. Environ.*, 316, 120188, <https://doi.org/10.1016/j.atmosenv.2023.120188>, 2024a.
- Cheng, J.-T. and Giordano, N.: Fluid flow through nanometer-scale channels, *Phys. Rev. E*, 65, 031206, <https://doi.org/10.1103/PhysRevE.65.031206>, 2002.
- Cheng, Y. L., Chen, L., Wu, H., Liu, J. Y., Ren, J. Y., and Zhang, F.: Wintertime fine aerosol particles composition and its evolution in two megacities of southern and northern China, *Sci. Total Environ.*, 914, <https://doi.org/10.1016/j.scitotenv.2023.169778>, 2024b.
- Cheung, H. C., Chou, C. C.-K., Lee, C. S. L., Kuo, W.-C., and Chang, S.-C.: Hygroscopic properties and cloud condensation nuclei activity of atmospheric aerosols under the influences of Asian continental outflow and new particle formation at a coastal site in eastern Asia, *Atmos. Chem. Phys.*, 20, 5911–5922, <https://doi.org/10.5194/acp-20-5911-2020>, 2020.
- Choi, C.-H. and Kim, C.-J.: Large slip of aqueous liquid flow over a nanoengineered superhydrophobic surface, *Phys. Rev. Lett.*, 96, 066001, <https://doi.org/10.1103/PhysRevLett.96.066001>, 2006.
- Churaev, N. V., Sobolev, V. D., and Somov, A. N.: Slippage of liquids over lyophobic solid surfaces, *J. Colloid Interface Sci.*, 97, 574–581, [https://doi.org/10.1016/0021-9797\(84\)90330-8](https://doi.org/10.1016/0021-9797(84)90330-8), 1984.
- Ciobanu, V. G., Marcolli, C., Krieger, U. K., Weers, U., and Peter, T.: Liquid–liquid phase separation in mixed organic/inorganic aerosol particles, *J. Phys. Chem. A*, 113, 10966–10978, <https://doi.org/10.1021/jp905054d>, 2009.
- Daellenbach, K. R., Kourtchev, I., Vogel, A. L., Bruns, E. A., Jiang, J., Petäjä, T., Jaffrezo, J.-L., Aksoyoglu, S., Kalberer, M., Baltensperger, U., El Haddad, I., and Prévôt, A. S. H.: Impact of anthropogenic and biogenic sources on the seasonal variation in the molecular composition of urban organic aerosols: a field and laboratory study using ultra-high-resolution mass spectrometry, *At-*

- mos. Chem. Phys., 19, 5973–5991, <https://doi.org/10.5194/acp-19-5973-2019>, 2019.
- Daellenbach, K. R., Cai, J., Hakala, S., Dada, L., Yan, C., Du, W., Yao, L., Zheng, F., Ma, J., Ungeheuer, F., Vogel, A. L., Stolzenburg, D., Hao, Y., Liu, Y., Bianchi, F., Uzu, G., Jaffrezo, J.-L., Worsnop, D. R., Donahue, N. M., and Kulmala, M.: Substantial contribution of transported emissions to organic aerosol in Beijing, *Nat. Geosci.*, 17, 747–754, <https://doi.org/10.1038/s41561-024-01493-3>, 2024.
- Davies, J. F. and Wilson, K. R.: Nanoscale interfacial gradients formed by the reactive uptake of OH radicals onto viscous aerosol surfaces, *Chem. Sci.*, 6, 7020–7027, <https://doi.org/10.1039/c5sc02326b>, 2015.
- El Haddad, I., Vienneau, D., Daellenbach, K. R., Modini, R., Slowik, J. G., Upadhyay, A., Vasilakos, P. N., Bell, D., de Hoogh, K., and Prevot, A. S. H.: Opinion: How will advances in aerosol science inform our understanding of the health impacts of outdoor particulate pollution?, *Atmos. Chem. Phys.*, 24, 11981–12011, <https://doi.org/10.5194/acp-24-11981-2024>, 2024.
- Freedman, M. A.: Phase separation in organic aerosol, *Chem. Soc. Rev.*, 46, 7694–7705, <https://doi.org/10.1039/C6CS00783J>, 2017.
- Freedman, M. A., Huang, Q., and Pitta, K. R.: Phase transitions in organic and organic/inorganic aerosol particles, *Annu. Rev. Phys. Chem.*, 75, 257–281, <https://doi.org/10.1146/annurev-physchem-083122-115909>, 2024.
- Gerrebos, N. G., Browning, L. P., Nikkho, S., Chartrand, E. R., Zaks, J., Wu, C., and Bertram, A. K.: Two-phase morphology and drastic viscosity changes in biomass burning organic aerosol after hydroxyl radical aging, *Environ. Sci. Atmos.*, <https://doi.org/10.1039/D5EA00084J>, 2025.
- Gerrebos, N. G. A., Zaks, J., Gregson, F. K. A., Walton-Raaby, M., Meeres, H., Zigg, I., Zandberg, W. F., and Bertram, A. K.: High viscosity and two phases observed over a range of relative humidities in biomass burning organic aerosol from Canadian wildfires, *Environ. Sci. Technol.*, 58, 21716–21728, <https://doi.org/10.1021/acs.est.4c09148>, 2024.
- Gkatzelis, G. I., Hohaus, T., Tillmann, R., Gensch, I., Müller, M., Eichler, P., Xu, K.-M., Schlag, P., Schmitt, S. H., Yu, Z., Wegener, R., Kaminski, M., Holzinger, R., Wisthaler, A., and Kiendler-Scharr, A.: Gas-to-particle partitioning of major biogenic oxidation products: a study on freshly formed and aged biogenic SOA, *Atmos. Chem. Phys.*, 18, 12969–12989, <https://doi.org/10.5194/acp-18-12969-2018>, 2018.
- Gou, Y., Xie, M., and Chen, J.: The phase state and viscosity of organic aerosol and related impacts on atmospheric physico-chemical processes: A review, *Atmos. Environ.*, 343, 120985, <https://doi.org/10.1016/j.atmosenv.2024.120985>, 2025.
- Grayson, J. W., Song, M., Sellier, M., and Bertram, A. K.: Validation of the poke-flow technique combined with simulations of fluid flow for determining viscosities in samples with small volumes and high viscosities, *Atmos. Meas. Tech.*, 8, 2463–2472, <https://doi.org/10.5194/amt-8-2463-2015>, 2015.
- Grayson, J. W., Zhang, Y., Mutzel, A., Renbaum-Wolff, L., Böge, O., Kamal, S., Herrmann, H., Martin, S. T., and Bertram, A. K.: Effect of varying experimental conditions on the viscosity of  $\alpha$ -pinene derived secondary organic material, *Atmos. Chem. Phys.*, 16, 6027–6040, <https://doi.org/10.5194/acp-16-6027-2016>, 2016.
- Gržinić, G., Bartels-Rausch, T., Berkemeier, T., Türler, A., and Ammann, M.: Viscosity controls humidity dependence of N<sub>2</sub>O<sub>5</sub> uptake to citric acid aerosol, *Atmos. Chem. Phys.*, 15, 13615–13625, <https://doi.org/10.5194/acp-15-13615-2015>, 2015.
- Guo, S., Hu, M., Zamora, M. L., Peng, J., Shang, D., Zheng, J., Du, Z., Wu, Z., Shao, M., Zeng, L., Molina, M. J., and Zhang, R.: Elucidating severe urban haze formation in China, *P. Natl. Acad. Sci. USA*, 111, 17373–17378, <https://doi.org/10.1073/pnas.1419604111>, 2014.
- Hallquist, M., Wenger, J. C., Baltensperger, U., Rudich, Y., Simpson, D., Claeys, M., Dommen, J., Donahue, N. M., George, C., Goldstein, A. H., Hamilton, J. F., Herrmann, H., Hoffmann, T., Iinuma, Y., Jang, M., Jenkin, M. E., Jimenez, J. L., Kiendler-Scharr, A., Maenhaut, W., McFiggans, G., Mentel, Th. F., Monod, A., Prévôt, A. S. H., Seinfeld, J. H., Surratt, J. D., Szmigielski, R., and Wildt, J.: The formation, properties and impact of secondary organic aerosol: current and emerging issues, *Atmos. Chem. Phys.*, 9, 5155–5236, <https://doi.org/10.5194/acp-9-5155-2009>, 2009.
- Ham, S., Babar, Z. B., Lee, J. B., Lim, H.-J., and Song, M.: Liquid–liquid phase separation in secondary organic aerosol particles produced from  $\alpha$ -pinene ozonolysis and  $\alpha$ -pinene photooxidation with/without ammonia, *Atmos. Chem. Phys.*, 19, 9321–9331, <https://doi.org/10.5194/acp-19-9321-2019>, 2019.
- Hinks, M. L., Brady, M. V., Lignell, H., Song, M., Grayson, J. W., Bertram, A. K., Lin, P., Laskin, A., Laskin, J., and Nizkorodov, S. A.: Effect of viscosity on photodegradation rates in complex secondary organic aerosol materials, *Phys. Chem. Chem. Phys.*, 18, 8785–8793, <https://doi.org/10.1039/C5CP05226B>, 2016.
- Hodzic, A., Campuzano-Jost, P., Bian, H., Chin, M., Colarco, P. R., Day, D. A., Froyd, K. D., Heinold, B., Jo, D. S., Katich, J. M., Kodros, J. K., Nault, B. A., Pierce, J. R., Ray, E., Schacht, J., Schill, G. P., Schroder, J. C., Schwarz, J. P., Sueper, D. T., Tegen, I., Tilmes, S., Tsigaridis, K., Yu, P., and Jimenez, J. L.: Characterization of organic aerosol across the global remote troposphere: a comparison of ATom measurements and global chemistry models, *Atmos. Chem. Phys.*, 20, 4607–4635, <https://doi.org/10.5194/acp-20-4607-2020>, 2020.
- Hosny, N., Fitzgerald, C., Vyšniauskas, A., Athanasiadis, A., Berkemeier, T., Uygur, N., Pöschl, U., Shiraiwa, M., Kalberer, M., and Pope, F.: Direct imaging of changes in aerosol particle viscosity upon hydration and chemical aging, *Chem. Sci.*, 7, 1357–1367, <https://doi.org/10.1039/C5SC02959G>, 2016.
- Hu, W., Hu, M., Hu, W.-W., Zheng, J., Chen, C., Wu, Y., and Guo, S.: Seasonal variations in high time-resolved chemical compositions, sources, and evolution of atmospheric submicron aerosols in the megacity Beijing, *Atmos. Chem. Phys.*, 17, 9979–10000, <https://doi.org/10.5194/acp-17-9979-2017>, 2017.
- Huang, Q., Pitta, K. R., Constantini, K., Ott, E.-J. E., Zuend, A., and Freedman, M. A.: Experimental phase diagram and its temporal evolution for submicron 2-methylglutaric acid and ammonium sulfate aerosol particles, *Phys. Chem. Chem. Phys.*, 26, 2887–2894, <https://doi.org/10.1039/D3CP04411D>, 2024.
- Huang, R. J., Zhang, Y. L., Bozzetti, C., Ho, K. F., Cao, J. J., Han, Y. M., Daellenbach, K. R., Slowik, J. G., Platt, S. M., Canonaco, F., Zotter, P., Wolf, R., Pieber, S. M., Bruns, E. A., Crippa, M., Ciarelli, G., Piazzalunga, A., Schwikowski, M., Abbazade, G., Schnelle-Kreis, J., Zimmermann, R., An, Z. S., Szidat, S., Baltensperger, U., El Haddad, I., and Prévôt,

- A. S. H.: High secondary aerosol contribution to particulate pollution during haze events in China, *Nature*, 514, 218–222, <https://doi.org/10.1038/nature13774>, 2014.
- Huang, Y., Mahrt, F., Xu, S., Shiraiwa, M., Zuend, A., and Bertram, A. K.: Coexistence of three liquid phases in individual atmospheric aerosol particles, *P. Natl. Acad. Sci. USA*, 118, e2102512118, <https://doi.org/10.1073/pnas.2102512118>, 2021.
- Jeon, J., Chen, Y., Kim, H., and Kim, Y. P.: Influences of meteorology on emission sources and physicochemical properties of particulate matter in Seoul, Korea during the heating period, *Atmos. Environ.*, 303, 119733, <https://doi.org/10.1016/j.atmosenv.2023.119733>, 2023.
- Jeong, R., Lilek, J., Zuend, A., Xu, R., Chan, M. N., Kim, D., Moon, H. G., and Song, M.: Viscosity and physical state of sucrose mixed with ammonium sulfate droplets, *Atmos. Chem. Phys.*, 22, 8805–8817, <https://doi.org/10.5194/acp-22-8805-2022>, 2022.
- Jimenez, J. L., Canagaratna, M. R., Donahue, N. M., Prevot, A. S. H., Zhang, Q., Kroll, J. H., DeCarlo, P. F., Allan, J. D., Coe, H., Ng, N. L., Aiken, A. C., Docherty, K. S., Ulbrich, I. M., Grieshop, A. P., Robinson, A. L., Duplissy, J., Smith, J. D., Wilson, K. R., Lanz, V. A., Hueglin, C., Sun, Y. L., Tian, J., Laaksonen, A., Raatikainen, T., Rautiainen, J., Vaattovaara, P., Ehn, M., Kulmala, M., Tomlinson, J. M., Collins, D. R., Cubison, M. J., E., Dunlea, J., Huffman, J. A., Onasch, T. B., Alfarra, M. R., Williams, P. I., Bower, K., Kondo, Y., Schneider, J., Drewnick, F., Borrmann, S., Weimer, S., Demerjian, K., Salcedo, D., Cottrell, L., Griffin, R., Takami, A., Miyoshi, T., Hatakeyama, S., Shimojo, A., Sun, J. Y., Zhang, Y. M., Dzepina, K., Kimmel, J. R., Sueper, D., Jayne, J. T., Herndon, S. C., Trimborn, A. M., Williams, L. R., Wood, E. C., Middlebrook, A. M., Kolb, C. E., Baltensperger, U., and Worsnop, D. R.: Evolution of organic aerosols in the atmosphere, *Science*, 326, 1525–1529, <https://doi.org/10.1126/science.1180353>, 2009.
- Jin, S., Huang, P., Park, J., Yoo, J. Y., and Breuer, K. S.: Near-surface velocimetry using evanescent wave illumination, *Exp. Fluids*, 37, 825–833, <https://doi.org/10.1007/s00348-004-0870-7>, 2004.
- Joseph, P. and Tabeling, P.: Direct measurement of the apparent slip length, *Phys. Rev. E*, 71, 035303, <https://doi.org/10.1103/PhysRevE.71.035303>, 2005.
- Kanakidou, M., Seinfeld, J. H., Pandis, S. N., Barnes, I., Dentener, F. J., Facchini, M. C., Van Dingenen, R., Ervens, B., Nenes, A., Nielsen, C. J., Swietlicki, E., Putaud, J. P., Balkanski, Y., Fuzzi, S., Horth, J., Moortgat, G. K., Winterhalter, R., Myhre, C. E. L., Tsigaridis, K., Vignati, E., Stephanou, E. G., and Wilson, J.: Organic aerosol and global climate modelling: a review, *Atmos. Chem. Phys.*, 5, 1053–1123, <https://doi.org/10.5194/acp-5-1053-2005>, 2005.
- Kiland, K. J., Mahrt, F., Peng, L., Nikkho, S., Zaks, J., Crescenzo, G. V., and Bertram, A. K.: Viscosity, glass formation, and mixing times within secondary organic aerosol from biomass burning phenolics, *ACS Earth Space Chem.*, 7, 1388–1400, <https://doi.org/10.1021/acsearthspacechem.3c00039>, 2023.
- Kim, H., Zhang, Q., Bae, G.-N., Kim, J. Y., and Lee, S. B.: Sources and atmospheric processing of winter aerosols in Seoul, Korea: insights from real-time measurements using a high-resolution aerosol mass spectrometer, *Atmos. Chem. Phys.*, 17, 2009–2033, <https://doi.org/10.5194/acp-17-2009-2017>, 2017.
- Kim, H., Zhang, Q., and Heo, J.: Influence of intense secondary aerosol formation and long-range transport on aerosol chemistry and properties in the Seoul Metropolitan Area during spring time: results from KORUS-AQ, *Atmos. Chem. Phys.*, 18, 7149–7168, <https://doi.org/10.5194/acp-18-7149-2018>, 2018.
- Kim, J. Y., Kim, Y. P., Yu, X., Yu, J., Wu, Z., Lee, H.-M., Song, M., Jang, K. S., Kim, C., Choi, N. R., and Lee, J. Y.: Concentrations and formation pathways of nitrogen-containing organic compounds in PM<sub>2.5</sub> from Seoul and Beijing, *Environ. Res.*, 286, 122959, <https://doi.org/10.1016/j.envres.2025.122959>, 2025.
- Kim, N., Kim, Y., Ghim, Y., Song, M., Kim, C., Jang, K., Lee, K., Shin, H., Jung, J., and Wu, Z.: Spatial distribution of PM<sub>2.5</sub> chemical components during winter at five sites in Northeast Asia: High temporal resolution measurement study, *Atmos. Environ.*, 290, 119359, <https://doi.org/10.1016/j.atmosenv.2022.119359>, 2022.
- Koop, T., Bookhold, J., Shiraiwa, M., and Pöschl, U.: Glass transition and phase state of organic compounds: dependency on molecular properties and implications for secondary organic aerosols in the atmosphere, *Phys. Chem. Chem. Phys.*, 13, 19238–19255, <https://doi.org/10.1039/c1cp22617g>, 2011.
- Kucinski, T. M., Ott, E.-J. E., and Freedman, M. A.: Dynamics of liquid–liquid phase separation in submicrometer aerosol, *J. Phys. Chem. A*, 125, 4446–4453, <https://doi.org/10.1021/acs.jpca.1c01985>, 2021.
- Kuwata, M. and Martin, S. T.: Phase of atmospheric secondary organic material affects its reactivity, *P. Natl. Acad. Sci. USA*, 109, 17354–17359, <https://doi.org/10.1073/pnas.1209071109>, 2012.
- Lam, H. K., Xu, R., Choczynski, J., Davies, J. F., Ham, D., Song, M., Zuend, A., Li, W., Tse, Y.-L. S., and Chan, M. N.: Effects of liquid–liquid phase separation and relative humidity on the heterogeneous OH oxidation of inorganic–organic aerosols: insights from methylglutaric acid and ammonium sulfate particles, *Atmos. Chem. Phys.*, 21, 2053–2066, <https://doi.org/10.5194/acp-21-2053-2021>, 2021.
- Li, J., Forrester, S. M., and Knopf, D. A.: Heterogeneous oxidation of amorphous organic aerosol surrogates by O<sub>3</sub>, NO<sub>3</sub>, and OH at typical tropospheric temperatures, *Atmos. Chem. Phys.*, 20, 6055–6080, <https://doi.org/10.5194/acp-20-6055-2020>, 2020.
- Li, K., Zhang, X., Zhao, B., Bloss, W. J., Lin, C., White, S., Yu, H., Chen, L., Geng, C., Yang, W., Azzi, M., George, C., and Bai, Z.: Suppression of anthropogenic secondary organic aerosol formation by isoprene, *npj Clim. Atmos. Sci.*, 5, 12, <https://doi.org/10.1038/s41612-022-00233-x>, 2022.
- Li, L., Mo, J., and Li, Z.: Flow and slip transition in nanochannels, *Physical Review E*, 90, 033003, <https://doi.org/10.1103/PhysRevE.90.033003>, 2014.
- Liu, J., Zhang, F., Ren, J., Chen, L., Zhang, A., Wang, Z., Zou, S., Xu, H., and Yue, X.: The evolution of aerosol mixing state derived from a field campaign in Beijing: implications for particle aging timescales in urban atmospheres, *Atmos. Chem. Phys.*, 25, 5075–5086, <https://doi.org/10.5194/acp-25-5075-2025>, 2025.
- Liu, S., Moffett, C. E., Vandergrift, G., Shrivastava, M., Cheng, Z., China, S., Nizkorodov, S. A., Zelenyuk, A., and Faiola, C. L.: Secondary organic aerosol from OH oxidation of acyclic terpenes is more viscous and less volatile than that of their cyclic analogs, *ACS ES&T Air*, 3, 83–94, <https://doi.org/10.1021/acsestair.5c00226>, 2026.

- Maclean, A. M., Smith, N. R., Li, Y., Huang, Y., Hettyadura, A. P. S., Crescenzo, G. V., Shiraiwa, M., Laskin, A., Nizkorodov, S. A., and Bertram, A. K.: Humidity-dependent viscosity of secondary organic aerosol from ozonolysis of  $\beta$ -caryophyllene: measurements, predictions, and implications, *ACS Earth Space Chem.*, 5, 305–318, <https://doi.org/10.1021/acsearthspacechem.0c00296>, 2021.
- Mahant, S., Iversen, E. M., Kasparoglu, S., Bilde, M., and Petters, M. D.: Direct measurement of the viscosity of ternary aerosol mixtures, *Environ. Sci. Atmos.*, 3, 595–607, <https://doi.org/10.1039/D2EA00160H>, 2023.
- Manavi, S. E. I., Aktypis, A., Siouti, E., Skyllakou, K., Myriokefalitakis, S., Kanakidou, M., and Pandis, S. N.: Atmospheric aerosol spatial variability: Impacts on air quality and climate change, *One Earth*, 8, <https://doi.org/10.1016/j.oneear.2025.101237>, 2025.
- Marshall, F. H., Berkemeier, T., Shiraiwa, M., Nandy, L., Ohm, P. B., Dutcher, C. S., and Reid, J. P.: Influence of particle viscosity on mass transfer and heterogeneous ozonolysis kinetics in aqueous–sucrose–maleic acid aerosol, *Phys. Chem. Chem. Phys.*, 20, 15560–15573, <https://doi.org/10.1039/C8CP01666F>, 2018.
- McNeill, V. F.: Atmospheric aerosols: clouds, chemistry, and climate, *Annu. Rev. Chem. Biomol. Eng.*, 8, 427–444, <https://doi.org/10.1146/annurev-chembioeng-060816-101538>, 2017.
- Meng, X., Wu, Z., Chen, J., Qiu, Y., Zong, T., Song, M., Lee, J., and Hu, M.: Particle phase state and aerosol liquid water greatly impact secondary aerosol formation: insights into phase transition and its role in haze events, *Atmos. Chem. Phys.*, 24, 2399–2414, <https://doi.org/10.5194/acp-24-2399-2024>, 2024.
- Mikhailov, E. F., Vlasenko, S. S., and Kiselev, A. A.: Water activity and surface tension of aqueous ammonium sulfate and D-glucose aerosol nanoparticles, *Atmos. Chem. Phys.*, 24, 2971–2984, <https://doi.org/10.5194/acp-24-2971-2024>, 2024.
- Nault, B. A., Jo, D. S., McDonald, B. C., Campuzano-Jost, P., Day, D. A., Hu, W., Schroder, J. C., Allan, J., Blake, D. R., Canagaratna, M. R., Coe, H., Coggon, M. M., DeCarlo, P. F., Diskin, G. S., Dunmore, R., Flocke, F., Fried, A., Gilman, J. B., Gkatzelis, G., Hamilton, J. F., Hanco, T. F., Hayes, P. L., Henze, D. K., Hodzic, A., Hopkins, J., Hu, M., Huey, L. G., Jobson, B. T., Kuster, W. C., Lewis, A., Li, M., Liao, J., Nawaz, M. O., Pollack, I. B., Peischl, J., Rappenglück, B., Reeves, C. E., Richter, D., Roberts, J. M., Ryerson, T. B., Shao, M., Sommers, J. M., Walega, J., Warneke, C., Weibring, P., Wolfe, G. M., Young, D. E., Yuan, B., Zhang, Q., de Gouw, J. A., and Jimenez, J. L.: Secondary organic aerosols from anthropogenic volatile organic compounds contribute substantially to air pollution mortality, *Atmos. Chem. Phys.*, 21, 11201–11224, <https://doi.org/10.5194/acp-21-11201-2021>, 2021.
- Nikkho, S., Bai, B., Mahrt, F., Zaks, J., Peng, L., Kiland, K. J., Liu, P., and Bertram, A. K.: Secondary organic aerosol from biomass burning phenolic compounds and nitrate radicals can be highly viscous over a wide relative humidity range., *Environ. Sci. Technol.*, 58, 21702–21715, <https://doi.org/10.1021/acs.est.4c06235>, 2024.
- Pöhlker, M. L., Pöhlker, C., Quaas, J., Mülmenstädt, J., Pozzer, A., Andreae, M. O., Artaxo, P., Block, K., Coe, H., Ervens, B., Gallimore, P., Gaston, C. J., Gunthe, S. S., Henning, S., Herrmann, H., Krüger, O. O., McFiggans, G., Poulain, L., Raj, S. S., Reyes-Villegas, E., Royer, H. M., Walter, D., Wang, Y., and Pöschl, U.: Global organic and inorganic aerosol hygroscopicity and its effect on radiative forcing, *Nat. Commun.*, 14, 6139, <https://doi.org/10.1038/s41467-023-41695-8>, 2023.
- Qiu, Y., Wu, Z., Man, R., Zong, T., Liu, Y., Meng, X., Chen, J., Chen, S., Yang, S., and Yuan, B.: Secondary aerosol formation drives atmospheric particulate matter pollution over megacities (Beijing and Seoul) in East Asia, *Atmos. Environ.*, 301, 119702, <https://doi.org/10.1016/j.atmosenv.2023.119702>, 2023.
- Rasool, Q. Z., Shrivastava, M., Liu, Y., Gaudet, B., and Zhao, B.: Modeling the impact of the organic aerosol phase state on multiphase OH reactive uptake kinetics and the resultant heterogeneous oxidation timescale of organic aerosol in the Amazon rainforest, *ACS Earth Space Chem.*, 7, 1009–1024, <https://doi.org/10.1021/acsearthspacechem.2c00366>, 2023.
- Reid, J. P., Bertram, A. K., Topping, D. O., Laskin, A., Martin, S. T., Petters, M. D., Pope, F. D., and Rovelli, G.: The viscosity of atmospherically relevant organic particles, *Nat. Commun.*, 9, <https://doi.org/10.1038/s41467-018-03027-z>, 2018.
- Renbaum-Wolff, L., Grayson, J. W., and Bertram, A. K.: Technical Note: New methodology for measuring viscosities in small volumes characteristic of environmental chamber particle samples, *Atmos. Chem. Phys.*, 13, 791–802, <https://doi.org/10.5194/acp-13-791-2013>, 2013a.
- Renbaum-Wolff, L., Grayson, J. W., Bateman, A. P., Kuwata, M., Sellier, M., Murray, B. J., Shilling, J. E., Martin, S. T., and Bertram, A. K.: Viscosity of  $\alpha$ -pinene secondary organic material and implications for particle growth and reactivity, *P. Natl. Acad. Sci. USA*, 110, 8014–8019, <https://doi.org/10.1073/pnas.1219548110>, 2013b.
- Rovelli, G., Song, Y.-C., Maclean, A. M., Topping, D. O., Bertram, A. K., and Reid, J. P.: Comparison of approaches for measuring and predicting the viscosity of ternary component aerosol particles, *Anal. Chem.*, 91, 5074–5082, <https://doi.org/10.1021/acs.analchem.8b05353>, 2019.
- Schnell, E.: Slippage of water over nonwetable surfaces, *J. Appl. Phys.*, 27, 1149–1152, <https://doi.org/10.1063/1.1722220>, 1956.
- Seinfeld, J. H., Bretherton, C. S., Carslaw, K. S., Coe, H., DeMott, P. J., Dunlea, E. J., Feingold, G., Ghan, S. J., Guenther, A., Kahn, R. A., Kraucunas, I., Kreidenweis, S. M., Molina, M. J., Nenes, A., Penner, J. E., Prather, K. A., Ramanathan, V., Ramaswamy, V., Rasch, P. J., Ravishankara, A. R., Rosenfeld, D., Stephens, G. L., and Wood, R.: Improving our fundamental understanding of the role of aerosol-cloud interactions in the climate system, *P. Natl. Acad. Sci. USA*, 113, 5781–5790, <https://doi.org/10.1073/pnas.1514043113>, 2016.
- Seong, C., Kim, D., Jeong, R., Qiu, Y. T., Wu, Z. J., Lee, J. Y., Lee, K. Y., Ahn, J., Jang, K. S., Zuend, A., Kim, C., Natsagdorj, A., and Song, M.: Influence of relative humidity and composition on PM phases in Northeast Asia, *ACS Earth Space Chem.*, 8, 788–797, <https://doi.org/10.1021/acsearthspacechem.4c00019>, 2024.
- Sheldon, C. S., Choczynski, J. M., Morton, K., Palacios Diaz, T., Davis, R. D., and Davies, J. F.: Exploring the hygroscopicity, water diffusivity, and viscosity of organic–inorganic aerosols – a case study on internally-mixed citric acid and ammonium sulfate particles, *Environ. Sci. Atmos.*, 3, 24–34, <https://doi.org/10.1039/d2ea00116k>, 2023.

- Shiraiwa, M. and Seinfeld, J. H.: Equilibration timescale of atmospheric secondary organic aerosol partitioning, *Geophys. Res. Lett.*, 39, <https://doi.org/10.1029/2012GL054008>, 2012.
- Shiraiwa, M., Ammann, M., Koop, T., and Pöschl, U.: Gas uptake and chemical aging of semisolid organic aerosol particles, *P. Natl. Acad. Sci. USA*, 108, 11003–11008, <https://doi.org/10.1073/pnas.1103045108>, 2011.
- Smith, N. R., Crescenzo, G. V., Huang, Y., Hettiyadura, A. P. S., Siemens, K., Li, Y., Faiola, C. L., Laskin, A., Shiraiwa, M., Bertram, A. K., and Nizkorodov, S. A.: Viscosity and liquid–liquid phase separation in healthy and stressed plant SOA, *Environ. Sci. Atmos.*, 1, 140–153, <https://doi.org/10.1039/D0EA00020E>, 2021.
- Son, J.-Y., Lee, J.-T., Kim, K.-H., Jung, K., and Bell, M. L.: Characterization of fine particulate matter and associations between particulate chemical constituents and mortality in Seoul, Korea, *Environ. Health Perspect.*, 120, 872, <https://doi.org/10.1289/ehp.1104316>, 2012.
- Song, M., Marcolli, C., Krieger, U. K., Zuend, A., and Peter, T.: Liquid-liquid phase separation in aerosol particles: Dependence on O:C, organic functionalities, and compositional complexity, *Geophys. Res. Lett.*, 39, 19801–19801, <https://doi.org/10.1029/2012gl052807>, 2012.
- Song, M., Marcolli, C., Krieger, U. K., Lienhard, D. M., and Peter, T.: Morphologies of mixed organic/inorganic/aqueous aerosol droplets, *Faraday Discuss.*, 165, 289–316, <https://doi.org/10.1039/c3fd00049d>, 2013.
- Song, M., Liu, P. F., Hanna, S. J., Li, Y. J., Martin, S. T., and Bertram, A. K.: Relative humidity-dependent viscosities of isoprene-derived secondary organic material and atmospheric implications for isoprene-dominant forests, *Atmos. Chem. Phys.*, 15, 5145–5159, <https://doi.org/10.5194/acp-15-5145-2015>, 2015.
- Song, M., Liu, P. F., Hanna, S. J., Zaveri, R. A., Potter, K., You, Y., Martin, S. T., and Bertram, A. K.: Relative humidity-dependent viscosity of secondary organic material from toluene photo-oxidation and possible implications for organic particulate matter over megacities, *Atmos. Chem. Phys.*, 16, 8817–8830, <https://doi.org/10.5194/acp-16-8817-2016>, 2016a.
- Song, M., Maclean, A. M., Huang, Y., Smith, N. R., Blair, S. L., Laskin, J., Laskin, A., DeRieux, W.-S. W., Li, Y., Shiraiwa, M., Nizkorodov, S. A., and Bertram, A. K.: Liquid–liquid phase separation and viscosity within secondary organic aerosol generated from diesel fuel vapors, *Atmos. Chem. Phys.*, 19, 12515–12529, <https://doi.org/10.5194/acp-19-12515-2019>, 2019.
- Song, M., Jeong, R., Kim, D., Qiu, Y., Meng, X., Wu, Z., Zuend, A., Ha, Y., Kim, C., Kim, H., Gaikwad, S., Jang, K.-S., Lee, J. Y., and Ahn, J.: Comparison of phase states of PM<sub>2.5</sub> over megacities, Seoul and Beijing, and their implications for particle size distribution, *Environ. Sci. Technol.*, 56, 17581–17590, <https://doi.org/10.1021/acs.est.2c06377>, 2022.
- Song, M., Li, Y., Seong, C., Yang, H., Jang, K.-S., Wu, Z., Lee, J. Y., Matsuki, A., and Ahn, J.: Direct observation of liquid–liquid phase separation and core–shell morphology of PM<sub>2.5</sub> collected from three Northeast Asian cities and implications for N<sub>2</sub>O<sub>5</sub> hydrolysis, *ACS ES&T Air*, 2, 1079–1088, <https://doi.org/10.1021/acsestair.5c00043>, 2025.
- Song, Y. C., Haddrell, A. E., Bzdek, B. R., Reid, J. P., Bannan, T., Topping, D. O., Percival, C., and Cai, C.: Measurements and predictions of binary component aerosol particle viscosity, *J. Phys. Chem. A.*, 120, 8123–8137, <https://doi.org/10.1021/acs.jpca.6b07835>, 2016b.
- Stewart, D. J., Cai, C., Nayler, J., Preston, T. C., Reid, J. P., Krieger, U. K., Marcolli, C., and Zhang, Y. H.: Liquid-liquid phase separation in mixed organic/inorganic single aqueous aerosol droplets, *J. Phys. Chem. A.*, 119, 4177–4190, <https://doi.org/10.1021/acs.jpca.5b01658>, 2015.
- Su, H., Cheng, Y., and Pöschl, U.: New multiphase chemical processes influencing atmospheric aerosols, air quality, and climate in the Anthropocene, *Acc. Chem. Res.*, 53, 2034–2043, <https://doi.org/10.1021/acs.accounts.0c00246>, 2020.
- Suda, S. R., Petters, M. D., Yeh, G. K., Strollo, C., Matsunaga, A., Faulhaber, A., Ziemann, P. J., Prenni, A. J., Carrico, C. M., Sullivan, R. C., and Kreidenweis, S. M.: Influence of functional groups on organic aerosol cloud condensation nucleus activity, *Environ. Sci. Technol.*, 48, 10182–10190, <https://doi.org/10.1021/es502147y>, 2014.
- Sun, J., Zhang, Q., Canagaratna, M. R., Zhang, Y., Ng, N. L., Sun, Y., Jayne, J. T., Zhang, X., Zhang, X., and Worsnop, D. R.: Highly time- and size-resolved characterization of submicron aerosol particles in Beijing using an Aerodyne Aerosol Mass Spectrometer, *Atmos. Environ.*, 44, 131–140, <https://doi.org/10.1016/j.atmosenv.2009.03.020>, 2010.
- Sun, Y., Luo, H., Li, Y., Zhou, W., Xu, W., Fu, P., and Zhao, D.: Atmospheric organic aerosols: online molecular characterization and environmental impacts, *npj Clim. Atmos. Sci.*, 8, 305, <https://doi.org/10.1038/s41612-025-01199-2>, 2025.
- Swietlicki, E., Hansson, H.-C., Hämeri, K., Svenningsson, B., Massling, A., McFiggans, G., McMurry, P. H., Petäjä, T., Tunved, P., and Gysel, M.: Hygroscopic properties of submicrometer atmospheric aerosol particles measured with H-TDMA instruments in various environments – a review, *Tellus B: Chem. Phys. Meteorol.*, 60, 432–469, <https://doi.org/10.1111/j.1600-0889.2008.00350.x>, 2008.
- Tan, F., Zhang, H., Xia, K., Jing, B., Li, X., Tong, S., and Ge, M.: Hygroscopic behavior and aerosol chemistry of atmospheric particles containing organic acids and inorganic salts, *npj Clim. Atmos. Sci.*, 7, 203, <https://doi.org/10.1038/s41612-024-00752-9>, 2024.
- Tao, J., Zhang, L., Cao, J., and Zhang, R.: A review of current knowledge concerning PM<sub>2.5</sub> chemical composition, aerosol optical properties and their relationships across China, *Atmos. Chem. Phys.*, 17, 9485–9518, <https://doi.org/10.5194/acp-17-9485-2017>, 2017.
- Tong, Y.-K., Liu, Y., Meng, X., Wang, J., Zhao, D., Wu, Z., and Ye, A.: The relative humidity-dependent viscosity of single quasi aerosol particles and possible implications for atmospheric aerosol chemistry, *Phys. Chem. Chem. Phys.*, 24, 10514–10523, <https://doi.org/10.1039/d2cp00740a>, 2022.
- Tretheway, D. C. and Meinhard, C. D.: Apparent fluid slip at hydrophobic microchannel walls, *Phys. Fluids*, 14, L9–L12, <https://doi.org/10.1063/1.1432696>, 2002.
- Ullah, A., Li, Y., and Song, M.: Temperature–RH dependent viscosity of organic aerosols from 273 to 303 K: implications for global N<sub>2</sub>O<sub>5</sub> uptake, *Atmos. Chem. Phys.*, 26, 2319–2329, <https://doi.org/10.5194/acp-26-2319-2026>, 2026.
- Ullmann, D. A., Hinks, M. L., Maclean, A. M., Butenhoff, C. L., Grayson, J. W., Barsanti, K., Jimenez, J. L., Nizkorodov,

- S. A., Kamal, S., and Bertram, A. K.: Viscosities, diffusion coefficients, and mixing times of intrinsic fluorescent organic molecules in brown limonene secondary organic aerosol and tests of the Stokes–Einstein equation, *Atmos. Chem. Phys.*, 19, 1491–1503, <https://doi.org/10.5194/acp-19-1491-2019>, 2019.
- Wall, C. J., Norris, J. R., Possner, A., McCoy, D. T., McCoy, I. L., and Lutsko, N. J.: Assessing effective radiative forcing from aerosol–cloud interactions over the global ocean, *P. Natl. Acad. Sci. USA*, 119, <https://doi.org/10.1073/pnas.2210481119>, 2022.
- Watanabe, K., Udagawa, Y., and Udagawa, H.: Drag reduction of Newtonian fluid in a circular pipe with a highly water-repellent wall, *J. Fluid Mech.*, 381, 225–238, <https://doi.org/10.1017/S0022112098003747>, 1999.
- Winston, P. W. and Bates, D. H.: Saturated Solutions For the Control of Humidity in Biological Research, *Ecology*, 41, 232–237, <https://doi.org/10.2307/1931961>, 1960.
- World Health Organization: WHO global air quality guidelines: particulate matter (PM<sub>2.5</sub> and PM<sub>10</sub>), ozone, nitrogen dioxide, sulfur dioxide and carbon monoxide, Geneva, ISBN 978-92-4-003422-8, 290 pp., 2021.
- You, Y., Renbaum-Wolff, L., and Bertram, A. K.: Liquid–liquid phase separation in particles containing organics mixed with ammonium sulfate, ammonium bisulfate, ammonium nitrate or sodium chloride, *Atmos. Chem. Phys.*, 13, 11723–11734, <https://doi.org/10.5194/acp-13-11723-2013>, 2013.
- Zaveri, R. A., Shilling, J. E., Zelenyuk, A., Zawadowicz, M. A., Suski, K., China, S., Bell, D. M., Veghte, D., and Laskin, A.: Particle-phase diffusion modulates partitioning of semivolatile organic compounds to aged secondary organic aerosol, *Environ. Sci. Technol.*, 54, 2595–2605, <https://doi.org/10.1021/acs.est.9b05514>, 2020.
- Zhang, J., Su, Y., Chen, C., Guo, W., Tan, Q., Feng, M., Song, D., Jiang, T., Chen, Q., Li, Y., Li, W., Wang, Y., Huang, X., Han, L., Wu, W., and Wang, G.: Chemical composition, sources and formation mechanism of urban PM<sub>2.5</sub> in Southwest China: a case study at the beginning of 2023, *Atmos. Chem. Phys.*, 24, 2803–2820, <https://doi.org/10.5194/acp-24-2803-2024>, 2024.
- Zhang, Q., Jimenez, J. L., Canagaratna, M. R., Allan, J. D., Coe, H., Ulbrich, I., Alfarra, M. R., Takami, A., Middlebrook, A. M., Sun, Y. L., Dzepina, K., Dunlea, E., Docherty, K., DeCarlo, P. F., Salcedo, D., Onasch, T., Jayne, J. T., Miyoshi, T., Shimojo, A., Hatakeyama, S., Takegawa, N., Kondo, Y., Schneider, J., Drewnick, F., Borrmann, S., Weimer, S., Demerjian, K., Williams, P., Bower, K., Bahreini, R., Cottrell, L., Griffin, R. J., Rautiainen, J., Sun, J. Y., Zhang, Y. M., and Worsnop, D. R.: Ubiquity and dominance of oxygenated species in organic aerosols in anthropogenically-influenced Northern hemisphere midlatitudes, *Geophys. Res. Lett.*, 34, <https://doi.org/10.1029/2007GL029979>, 2007.
- Zhang, Y., Tang, L., Croteau, P. L., Favez, O., Sun, Y., Canagaratna, M. R., Wang, Z., Couvidat, F., Albinet, A., Zhang, H., Sciare, J., Prévôt, A. S. H., Jayne, J. T., and Worsnop, D. R.: Field characterization of the PM<sub>2.5</sub> Aerosol Chemical Speciation Monitor: insights into the composition, sources, and processes of fine particles in eastern China, *Atmos. Chem. Phys.*, 17, 14501–14517, <https://doi.org/10.5194/acp-17-14501-2017>, 2017.
- Zhao, J., Qiu, Y. M., Zhou, W., Xu, W. Q., Wang, J. F., Zhang, Y. J., Li, L. J., Xie, C. H., Wang, Q. Q., Du, W., Worsnop, D. R., Canagaratna, M. R., Zhou, L. B., Ge, X. L., Fu, P. Q., Li, J., Wang, Z. F., Donahue, N. M., and Sun, Y. L.: Organic aerosol processing during winter severe haze episodes in Beijing, *J. Geophys. Res.-Atmos.*, 124, 10248–10263, <https://doi.org/10.1029/2019jd030832>, 2019.
- Zhou, S., Shiraiwa, M., McWhinney, R. D., Pöschl, U., and Abbatt, J. P.: Kinetic limitations in gas–particle reactions arising from slow diffusion in secondary organic aerosol, *Faraday Discuss.*, 165, 391–406, <https://doi.org/10.1039/C3FD00030C>, 2013.
- Zhou, W., Xu, W., Kim, H., Zhang, Q., Fu, P., Worsnop, D. R., and Sun, Y.: A review of aerosol chemistry in Asia: insights from aerosol mass spectrometer measurements, *Environ. Sci. Process. Impacts*, 22, 1616–1653, <https://doi.org/10.1039/D0EM00212G>, 2020.
- Zhu, L., Neto, C., and Attard, P.: Reliable measurements of interfacial slip by colloid probe atomic force microscopy. III. Shear-rate-dependent slip, *Langmuir*, 28, 3465–3473, 2012.
- Zobrist, B., Marcolli, C., Pedernera, D. A., and Koop, T.: Do atmospheric aerosols form glasses?, *Atmos. Chem. Phys.*, 8, 5221–5244, <https://doi.org/10.5194/acp-8-5221-2008>, 2008.
- Zuend, A. and Seinfeld, J. H.: Modeling the gas–particle partitioning of secondary organic aerosol: the importance of liquid–liquid phase separation, *Atmos. Chem. Phys.*, 12, 3857–3882, <https://doi.org/10.5194/acp-12-3857-2012>, 2012.